
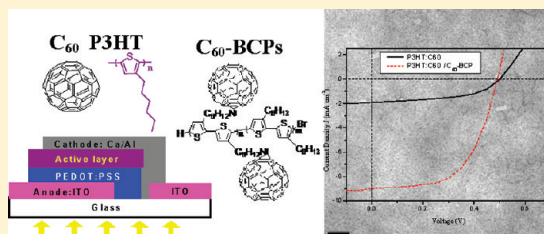


Highly Efficient P3HT: C₆₀ Solar Cell Free of Annealing ProcessShu-Hua Chan,^{*,†,‡} Chia-Sheng Lai,[‡] Hsin-Lung Chen,[‡] Ching Ting,[§] and Chih-Ping Chen^{*,†}[†]Materials and Chemical Laboratories, Industrial Technology Research Institute, 195, Sec. 4, Chung Hsing Road, Chutung, Hsinchu, 310, Taiwan[‡]Department of Chemical Engineering, National Tsing Hua University, Hsin-Chu 30013, Taiwan[§]Advance Technology Project Division, DelSolar Corporation, 2 R&D second Road, Science-Based Industrial Park, HsinChu 30076, Taiwan Supporting Information

ABSTRACT: All conjugated C₆₀-containing block copolymers (BCPs) based on quasi-living Grignard metathesis (GRIM) polymerization have been designed and synthesized for application in polymer solar cells (PSCs). The C₆₀-containing BCP can induce the formation of a self-organization nanostructure of P3HT domain. Moreover, this C₆₀-containing BCP serves as a compatibilizer to reduce the interfacial tension between the P3HT and C₆₀, thus help establishing a moderate phase-separated morphology with crystalline P3HT and C₆₀ domain. The performance up to 2.56% (AM 1.5G irradiation (100 mW/cm²)) of a P3HT:C₆₀ device can be achieved by using C₆₀-BCP as additive without any post-treatment.



INTRODUCTION

Polymer bulk-heterojunction (BHJ) solar cells have drawn scientific interests due to their potential as low-cost energy sources.¹ One of the critical factors to further improve device performance is the well-defined morphologies of blended donor (D) and acceptor (A) moieties, in which they provide suitable interfaces for exciton dissociation and have the preferred carrier pathways connected to the corresponding electrodes. Several techniques including solvent² or thermal annealing,³ varying the composition of the processing solvent mixture and additives,⁴ and chemical structure variation of the active materials⁵ have been identified experimentally for effective manipulation of the morphology of the blend films and, hence, improvement of the performance of BHJ solar cells. These process conditions affect the intercorrelated factors that determine the phase behavior of blend films. For instance, the Flory-Huggins parameter and solubility of the D and A materials, as well as the kinetic factors involved in the solvent evaporation, the thermal post-treatment, and crystallization processes all play a key role on the morphology control of the active layer.

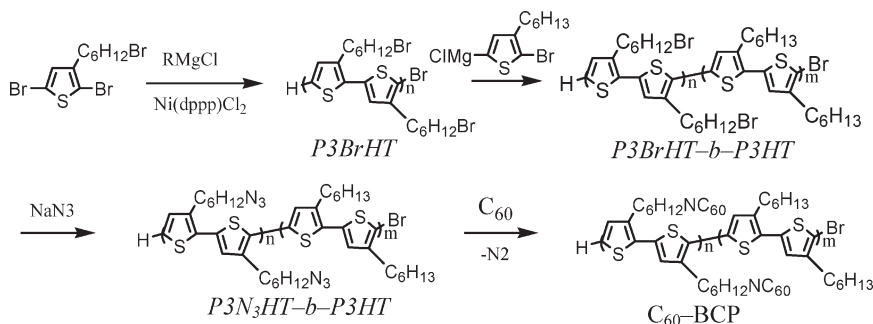
For a straightforward cell fabrication, the blends need to be self-organized into a well-defined nano-scaled morphology during the time scale of film formation. Herein, we report a new concept to well control the phase separation in BHJ cell by incorporating all-conjugated block copolymers (BCPs) besides active materials during active layer formation. This protocol circumvents the need of additional post-treatment step and the detrimental device performance often associated with the additives residue. There have been several reports on the self-assembly behavior of conjugated diblock polymer contained in BCPs.⁶ The immiscibility or the crystallinity difference between

two blocks resulted in 3-dimensional microphase-separated patterns. However, the introduction of those insulating blocks in previous studies dilutes the concentration of the semiconducting materials in the films, leading to a decline in their electronic conductivity. Recently, Tajima et al. reported the synthesis of an all-conjugated BCP via quasi-living polymerization,⁷ and interesting morphologies, which showed partly aligned worm-like structure, were found on their regioregular poly[(3-hexylthiophene)-*block*-(3-(2-ethylhexyl)thiophene)] copolymers. Here we demonstrate the synthesis of a novel all conjugated C₆₀-containing BCP by quasi-living Grignard metathesis (GRIM) polymerization (Scheme 1). Furthermore, BCP have previously been used as compatibilizers for blend of immiscible materials.⁸ In these systems, confinement of BCP joints at domain interfaces modifying domain sizes and blend morphology. The use of BCP as compatibilizer in controlling the large scale phase separation within blends of P3HT and perylene tetracarboxydiimide (PDI) have been demonstrated by Fréchet et al.^{8a} As their result, solar cell performance was enhanced in the presence of 25% (mass) BCP as compatibilizer. In our study, the C₆₀-containing BCP serves as a compatibilizer to reduce the interfacial tension between the P3HT and C₆₀, thus helping to establish a moderate phase-separated morphology with crystalline P3HT and C₆₀ domains. Moreover, BCP offers the tendency to induce self-organization of P3HT domains and thus enhances hole molecular mobility.

Received: June 22, 2011

Revised: September 28, 2011

Published: October 25, 2011

Scheme 1. Synthesis Route of C₆₀-BCP

RESULTS AND DISCUSSION

The synthesis of P3C₆₀HT-*b*-P3HT (C₆₀-BCP) involves a transformation process start with quasi-living chain growth polymerization⁹ of 2,5-dibromo-3-hexylthiophene and 2,5-dibromo-6-bromo-3-hexylthiophene, followed by incorporation of C₆₀ as substitutes to the second block by azido functional group.^{10,11} (Scheme 1) The success of C₆₀-BCP synthesis depends on the polymerization time control and the tolerance of functionality. As a result of gel permeation chromatography (GPC) (Figure S1, Supporting Information), the P3BrHT peaks shift to high molecular weight (P3BrHT-*b*-P3HT) with the maintenance of the one-peak shape. The number-average molecular weight (*M_n*) of P3BrHT-*b*-P3HT is 10693 with narrow PDIs of 1.07. These results indicate the successful synthesis of the P3BrHT-*b*-P3HT by quasi-living GRIM polymerization. The ¹H NMR spectrum of P3BrHT-*b*-P3HT is shown in Figure S2(a), Supporting Information. The peak observed at 6.90 ppm could be assigned to the sp² CH of thiophene rings and the peak at 2.57 and 2.81 ppm to the sp³ CH₂ attached to the thiophene rings in the P3HT and P3BrHT fractions. The peaks in the ranges of δ 1.35–1.95 ppm arise from methylene groups of P3BrHT-*b*-P3HT. The peaks observed at δ 3.44 ppm could be assigned to the CH₂Br of P3BrHT fractions, and 0.9 ppm to the methyl group of P3HT fractions. From the integration of the peaks in both regions, the molar ratios of the P3HT and P3BrHT segments was 87:13, which was close to the feed molar ratio of 85:15. The newly ¹H NMR peaks at 3.29 ppm arises from the methylene attached to the azide group which, indicates the successful transfer of P3BrHT to P3N₃HT. (Figure S2(b), Supporting Information) As shown in Figure S2(c), Supporting Information, the signal of the azide intermediate at 3.29 ppm disappeared after reaction with C₆₀, while the intensity of peaks around 2.57 ppm increased. All the integral ratios of peak areas agree with the corresponding molecular structure of the polymers. In addition, the UV–vis spectrum of the C₆₀-BCP in chloroform solution shows dominant centered at 413 nm with a shoulder band at 330 nm. The high-energy band reflects the absorption of C₆₀ units and the low energy absorption is attributed to P3HT segment (see comparison to UV–vis spectrum between P3BrHT-*b*-P3HT and P3C₆₀HT-*b*-P3HT, Figure S3, Supporting Information). Both observations indicate the covalent attachment of C₆₀ to the polymer.

The thin film property of C₆₀-BCP was first examined by AFM tapping mode. As shown in Figure 1a, fiber-like structures are observed throughout of C₆₀-BCP film. On the basis of previous study of C₆₀ contained block copolymers, it is likely that the P3HT segment forms the fibers (bright regions) while

the P3C₆₀HT blocks assemble on side of the fiber (dark regions).¹² It is well-known that P3HT can self-assemble to well-defined nanostructure. This behavior can be recognized by UV–vis absorption at specific wavelengths. As shown in Figure 1b, four absorption peaks located at 330, 515, 550, and 610 nm can be observed for C₆₀-BCP thin film. The spectrum at 330 nm is denoted to the absorption of C₆₀. The residue peaks were attributed to the P3HT absorption peaks and are known to be related to the vibronic splitting of the π – π^* transition, and their degree of polymer ordering. The absorption peak appeared at 610 nm is associated with the interchain π – π^* transition of P3HT and reflects a significant degree of structural ordering. The crystallinity of the C₆₀-BCP was further verified by WAXD measurements. The films for WAXD were made by casting from dichlorobenzene solution. As shown in Figure 1c, the diffraction profile associated with C₆₀-BCP shows a characteristic of P3HT crystals, the diffraction peaks at $q = 2.8, 5.6,$ and 8.4 nm^{-1} , which are assigned to the reflections of crystallographic (1 0 0), (2 0 0), and (3 0 0) planes of P3HT segment crystals, respectively.^{12,13} The scattering vector can be identified as corresponding to real-space d value of 2.28 nm associated with the interlayer spacing of P3HT block. The broad peak from 8 to 12 nm^{-1} reveals the amorphous parts of C₆₀-BCP domains.

By coupling the P3C₆₀HT to incompatible P3HT segments, the fibrillar morphology was found. We further examine the self-organizing behavior of the P3HT with the presence of the C₆₀-BCP. For direct comparison, we prepared the films for tapping mode AFM analysis under the same conditions without any post-treatment. Figure 2 displays the phase images of P3HT: C₆₀-BCP blend films with various ratio of C₆₀-BCP added. The morphology in the blend film changes dramatically upon the presence of C₆₀-BCP. Pristine P3HT film was rather smooth and featureless, while the blend film with 20% C₆₀-BCP showed the fibrillar structure. This effect becomes more pronounced when the ratio of C₆₀-BCP in the blend increases, as even larger fibril-like nanostructure is observed with 30% C₆₀-BCP blend film (Figure 2c). The obtained structure is the result of self-assemble behavior interplay between π – π^* stacking and phase separation. The present of C₆₀-BCP facilitates the self-assemble of P3HT. The solid-state UV–vis absorption spectra provide supporting evidence for self-organization of P3HT domains in Figure 3. The growth of three vibronic shoulders (at 515, 550, and 610 nm) due to strong interchain–interlayer interactions or better packing of P3HT suggests that the morphology of P3HT gradually shifts from semicrystalline to more crystalline when C₆₀-BCP is added.

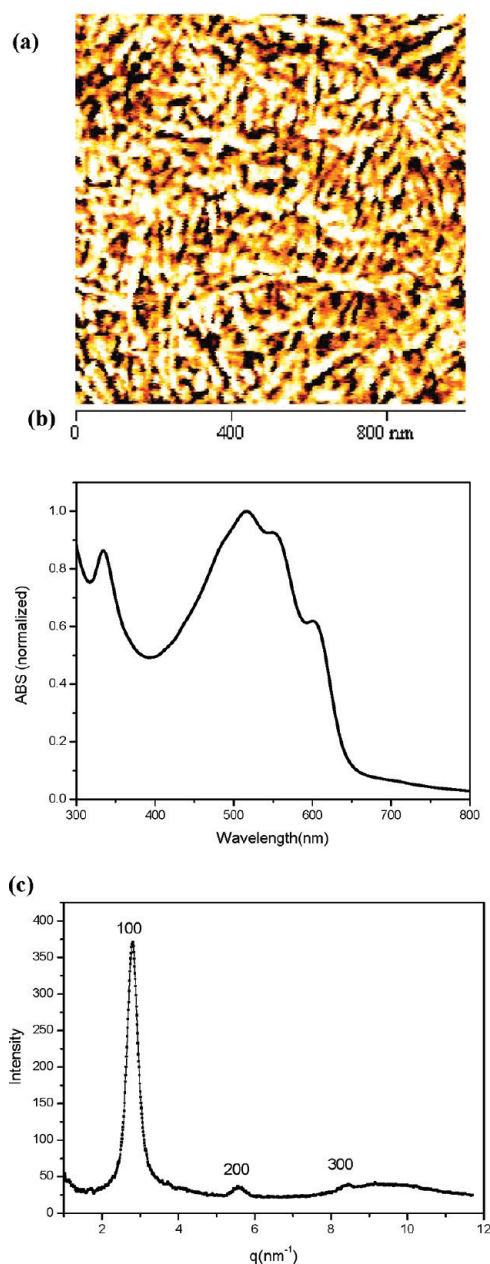


Figure 1. AFM phase image (a), UV-vis spectrum (b), and WAXD pattern (c) of C_{60} -BCP film.

Although plain C_{60} offers great cost-effective advantage, however, it is also well acknowledged that the limitation of C_{60} manipulation results from its poor solubility in common solvents and its tendency to crystallize. Because of these properties, well-defined C_{60} blends morphology are usually difficult to obtain,¹⁴ thus, the high performance P3HT: C_{60} devices often requires delicate post-treatment,¹⁵ which usually requires long processing times (tens of minutes for thermal annealing¹⁶ or a few hours for solvent annealing¹⁷). To emphasize the main purpose of study, we used P3HT as the donor and C_{60} as the acceptor for the fabricating solar cell to demonstrate the effect of C_{60} -BCP in BHJ system. The devices take the structure of indium tin oxide (ITO)/PEDOT: PSS/P3HT: C_{60} with C_{60} -BCP/Ca/Al using methods similar to those we reported previously.¹⁴ Figure 4 shows the I - V curves of

the PSCs under the condition of AM 1.5 at 100 mW/cm². Representative characteristics of the solar cells are listed in Table 1.

We monitored the device performance with P3HT-to- C_{60} -BCP ratio to determine the optimal composition. Table 1 and Figure 4 reveal that the optimal C_{60} -BCP ratios fell around 20 wt %. Upon further increasing the C_{60} -BCP content, both J_{sc} and the FF of the cell decreased. Our best performing device was fabricated by spin-casting a blend solution with a concentration of 20 mg/mL (P3HT: C_{60} = 1:0.5) at a spin rate of 450 rpm for 30 s, with DCB as the solvent and 20% C_{60} -BCP incorporated. This device exhibited a PCE of 2.56% under AM 1.5 G irradiation (100 mW/cm²), with J_{sc} , V_{oc} , and FF of the resulting device being 9.0 mA/cm², 0.49 V, and 0.58, respectively. In comparison with the P3HT: C_{60} device, the photocurrent underwent a significant increase of ca. 450%. We estimated the series resistance (R_s) and shunt resistance (R_{sh}) from the inverse slope of the J - V curve. A significant decrease of R_s from 35 to 11 Ω /cm² is obtained after using the C_{60} -BCP, which implies the bulk resistance of devices is lower. The R_{sh} values of P3HT: C_{60} and C_{60} -BCP (749 Ω /cm²) derived devices were 832 and 749 Ω /cm², respectively. The similar R_{sh} result indicates that the interface defects caused charge recombination and leakage current is not the dominative factor. It is also known that the hole mobility of active layer needs to be higher for effective carrier transport and will directly affects the device performance. A hole-only device structure is adopted to extract and compare the hole mobilities of blend films in both systems.¹⁷ The estimated field-independent mobility of the P3HT: C_{60} and C_{60} -BCP derived devices are 2.2×10^{-9} m²/(V s) and 7.8×10^{-9} m²/(V s), respectively. As expected, the hole mobility of C_{60} -BCP derived device shows nearly 4 times higher than P3HT: C_{60} only device which enables the better carrier transport within active layer and, hence, a higher attainable J_{sc} . The enhanced charge mobility indicates more ordered and crystallinity of P3HT as suggested from AFM and UV-vis data. The increase in the carrier mobility accomplishes the reduction of the recombination process of hole-electron pairs, hence leading to an increase in the short-circuit current (J_{sc}).¹⁸ The simulation model has also shown that to attain a large mean carrier distance, which leads to high J_{sc} , carrier mobility should be large.¹⁹ Figure 5 displays the TEM images of P3HT: C_{60} and C_{60} -BCP derived devices for direct comparison of the morphology of the active layer processed using C_{60} -BCP. We attribute the dark areas to the C_{60} domains for its higher electron scattering density than that of the conjugated polymer.²⁰ Figure 5b reveals a uniform blend of C_{60} surrounded by P3HT domains from C_{60} -BCP derived film while the P3HT: C_{60} blend (Figure 5a) exhibits a larger C_{60} aggregation clusters. Unsatisfactory OPV performance for P3HT: C_{60} is drastically associated with its microphase separation. For shorter exciton diffusion lengths (<20 nm), free carrier will be limited by large C_{60} clusters (>500 nm) and, consequently, cause lower device performance.^{4b} In films with C_{60} -BCP, such behavior is largely suppressed and smaller domains are observed. This result indicates that the improved PCE was mainly due to spatial distribution of the D/A domains. It is apparent that a moderate phase-separated morphology induced by C_{60} -BCP incorporation would enhance carrier transport within a cell.

CONCLUSIONS

In summary, all-conjugated C_{60} -BCP were synthesized by quasi-living GRIM polymerization in a well-controlled fashion.

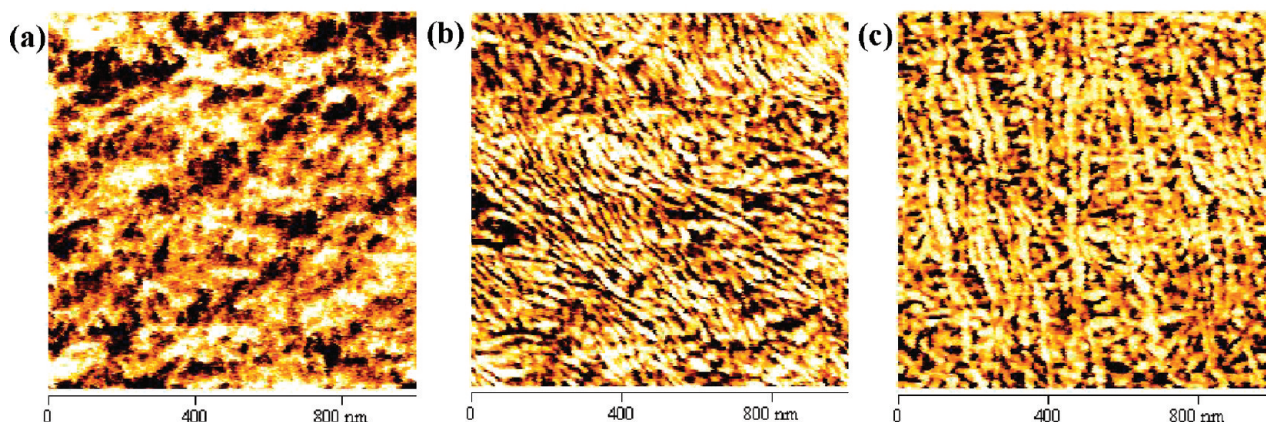


Figure 2. AFM phase images of P3HT: C_{60} -BCP blended films from different ratios of C_{60} -BCP: (a) P3HT, (b) 20% of C_{60} -BCP, and (c) 30% of C_{60} -BCP.

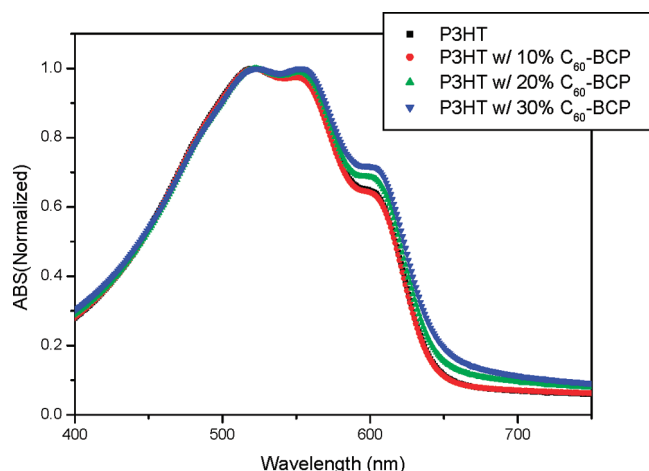


Figure 3. UV-vis spectra of P3HT: C_{60} -BCP blend films from different ratios: pure P3HT film (\square), 10% C_{60} -BCP film (\circ), 20% C_{60} -BCP film (Δ), and 30% C_{60} -BCP film (∇).

The incorporation of P3HT with C_{60} -BCP can induce the formation of a self-organization nanostructure and enhance the interchain interactions of P3HT domain. An efficient polymer solar cell (2.56% under AM 1.5G 100 mW/cm²) based on P3HT: C_{60} = 1:0.5 with 20% diblock copolymer is demonstrated. We infer that a moderate phase-separated morphology with crystalline P3HT and C_{60} domains in active layer is the key to a high photocurrent because it is advantageous for both carrier separation and transport. This study highlights the importance of a facile route for morphology control driven by BCP, as well as to understand the effects of BCP serving as a compatibilizer among the active layer and how it yields higher-performance devices without post-treatment.

EXPERIMENTAL DETAILS

General Measurement and Characterization. All chemicals are purchased from Aldrich and used as received unless otherwise specified. ¹H spectra were measured using Bruker 500 MHz instrument spectrometers. Absorption spectra were taken on a PerkinElmer Lambda 950 UV-vis spectrophotometer. The molecular weight of polymers was measured by the GPC method (Waters), and polystyrene

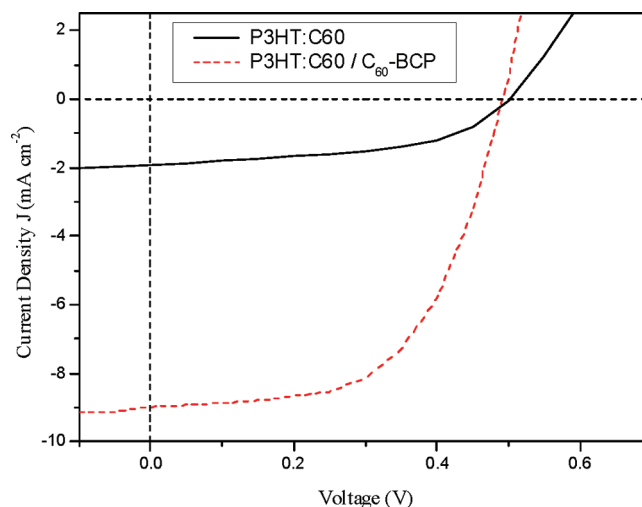
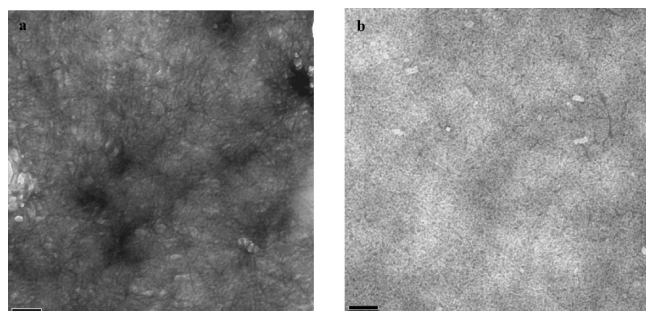


Figure 4. Current density-potential characteristics of P3HT: C_{60} and P3HT: C_{60} / C_{60} -BCP devices under illumination with AM 1.5G simulated solar light (100 mW/cm²).

was used as the standard (THF as the eluent). The morphology of the polymer films was analyzed by atomic force microscopy (AFM; VEECO DCP-II) with the dynamic force mode at ambient temperature. An etched Si probe under resonant frequency of 90 kHz and spring constants of 11 N/m was used. WAXD profiles were obtained by using a by using a Shimadzu XD-5 X-ray diffractometer with fixed X-ray wavelength of 1.542 Å. All the bulk-heterojunction photovoltaic cells were prepared using the same preparation procedures and device fabrication procedure referring as following: The glass-indium tin oxide (ITO) substrates (obtained from Sanyo, Japan (8Ω/□)) were first patterned by lithograph, then cleaned with detergent, and ultrasonicated in acetone and isopropyl alcohol, and subsequently dried on hot plate at 120 °C for 5 min, and finally treated with oxygen plasma for 5 min. Poly(3,4-ethylenedioxythiophene):poly(styrene sulfonate) (PEDOT:PSS, Baytron P-VP A14083) was filtered through a 0.45 μm filter before being deposited on ITO with a thickness around 30 nm by spin coating at 3000 rpm in the air and dried at 150 °C for 30 min inside glovebox. The thin films of P3HT: C_{60} (1:0.5 w/w) were made by spin coating from 450 rpm on the top of PEDOT:PSS layer from 20 mg/mL dichlorobenzene solution. Subsequently the device was completed by coating 30 nm thickness of Ca and an 80 nm thickness of Al

Table 1. Performance Comparison of P3HT/C₆₀ Blend Films with Different Ratios of C₆₀–BCP

P3HT:C ₆₀	<i>J</i> _{sc} (mA/cm ²)	<i>V</i> _{oc} (V)	FF	PCE (%)
w/o BCPs	1.9	0.50	0.51	0.48
10% BCPs	9.2	0.47	0.56	2.42
20% BCPs	9.0	0.49	0.58	2.56
30% BCPs	8.4	0.49	0.51	2.10

**Figure 5.** TEM images of (a) P3HT:C₆₀ and (b) P3HT:C₆₀ with 20% C₆₀–BCP. The scale bar is 500 nm.

in $<10^{-6}$ Torr pressure, respectively. The active area of the device is 5 mm². Finally the cell was encapsulated using UV-curing glue (purchased from Nagase, Japan). After encapsulation, all devices measurements were operated in an ambient atmosphere at 25 °C. I–V curves of the OPV devices were measured using a computer-controlled Keithley 2400 source measurement unit (SMU) equipped with a Peccell solar simulator under AM 1.5G illumination (100 mW cm^{−2}). The illumination intensity was calibrated using a standard Si photodiode detector equipped with a KG-5 filter. The output photocurrent was adjusted to match the photocurrent of the Si reference cell to obtain a power density of 100 mW cm^{−2}. The efficiency of 3.5% of a P3HT/PCBM reference cell measured under illumination in our laboratory was verified to be 3.4% under AM1.5G conditions (100 mW cm^{−2}) in National Institute of Advanced Industrial Science and Technology (AIST, Japan).

Synthesis of P3BrHT-*b*-P3HT. 2,5-Dibromo-3-hexylthiophene-(3-HT) and 2,5-dibromo-6-bromo-3-hexylthiophene(3BrHT) were synthesized following the literature method.¹⁰ The synthesis procedure of P3BrHT-*b*-P3HT (feed molar ratio of 0.15:0.85) was as follows: two round bottomed flasks (100 mL) equipped with a two-neck stopcock were dried by heating under reduced pressure and cooled to room temperature. 3BrHT (0.5 g, 1.2 mmol) was placed in one flask under N₂ and then evacuated under reduced pressure to remove moisture and oxygen. After anhydrous THF (45 mL) was added, the solution was stirred at 0 °C. A 2 M solution of *tert*-butyl-MgCl in THF (0.7 mL, 1.4 mmol) was added, and the mixture was stirred at room temperature for 30 min (solution 1). In the other flask, 3-HT (2.4 g, 7 mmol) was first reacted with *tert*-BuMgCl (3.5 mL, 7 mmol) (solution 2) at room temperature for 30 min, and then heated to 50 °C. Solution 1 was heated up to 50 °C and Ni(dppe)Cl₂ catalyst (21.7 mg, 0.041 mmol) was added in one portion. After being stirred for 1 h (the *M*_n of precursor (P3BrHT) is around 2636; see Figure S2, Supporting Information), solution 2 was transferred to solution 1, and the resulting solution was stirred at 50 °C for 6 h. Finally, the reaction was quenched by adding HCl solution (10 wt %). The crude polymer was successively washed by Soxhlet extraction using methanol, acetone, and hexane to give a purple solid (83% yield): *M*_w (11222 g/mol), *λ*_{max} = 428 nm (CHCl₃).

Synthesis of P3N₃HT-*b*-P3HT¹⁰. P3BrHT-*b*-P3HT (490 mg) was dissolved in DMF(100 mL), then sodium azide (1.3 g, 20 mmol)

was added in one portion, and the resulting mixture was stirred and reflux overnight. The reaction was quenched in methanol. The solid polymer was washed with methanol by using a Soxhlet extractor. The polymer was dissolved with CHCl₃ and precipitated with MeOH to give a solid polymer. (yield 90%) The ¹H NMR spectrum of P3N₃HT-*b*-P3HT is shown in Figure S2, Supporting Information. All the integral ratios of peak areas agree with the corresponding molecular structure of the polymers: *M*_w (11852 g/mol); *λ*_{max} = 428 nm (CHCl₃).

Synthesis of P3C₆₀HT-*b*-P3HT. The corresponding P3N₃HT-*b*-P3HT and C₆₀ (2 equiv relative to the amount of N₃HT segment) were dissolved in chlorobenzene and degassed by bubbling with dry N₂ for 15 min.¹⁰ The mixture was stirred at 100 °C for overnight. After cooling to room temperature, the organic layer was washed with water, dried over Na₂SO₄, and concentrated to remove the solvent. The residue was diluted with THF (500 mL), filtered, and washed until a colorless filtrate, and the THF was removed under reduced pressure. After repeating this latter step, the polymer was precipitated in methanol (200 mL), and the final product was dried under reduced pressure (70 °C, 16 h) (yield 81%): *M*_w (21479 g/mol); *λ*_{max} = 408 nm (CHCl₃)

■ ASSOCIATED CONTENT

S Supporting Information. ¹H NMR, GPC, and UV–vis spectra of materials are included in Supporting Information. This material is available free of charge via the Internet at <http://pubs.acs.org>.

■ AUTHOR INFORMATION

Corresponding Author

*E-mail: (S.-H.C.) Shu_Hua_Chan@itri.org.tw; (C.-P.C.) chiiping_chen@itri.org.tw. Telephone: 886-35-913588. Fax: 886-35-827694.

■ ACKNOWLEDGMENT

We thank the Ministry of Economic Affairs, Taiwan, for financial support.

■ REFERENCES

- (1) (a) Helgesen, M.; Søndergaard, R.; Krebs, F. C. *J. Mater. Chem.* **2010**, *20*, 36. (b) Thompson, B. C.; Fréchet, J. M. J. *Angew. Chem., Int. Ed.* **2008**, *47*, 58. (c) Krebs, F. C. *Sol. Energy Mater. Sol. Cells* **2009**, *93*, 465. (d) Helgesen, M.; Søndergaard, R.; Krebs, F. C. *J. Mater. Chem.* **2010**, *20*, 36. (e) Krebs, F. C.; Gevorgyan, S. A.; Alstrup, J. *J. Mater. Chem.* **2009**, *19*, 5442.
- (2) (a) Li, G.; Shrotriya, V.; Huang, J.; Yao, Y.; Moriarty, T.; Kimerly, K.; Yang, Y. *Nat. Mater.* **2005**, *4*, 864. (b) Chen, Y.-C.; Yu, C.-Y.; Fan, Y.-L.; Hung, L.-I.; Chen, C.-P.; Ting, C. *Chem. Commun.* **2010**, *46*, 6503.
- (3) (a) Ma, W. L.; Yang, C. Y.; Gong, X.; Lee, K.; Heeger, A. J. *Adv. Funct. Mater.* **2005**, *15*, 1617. (b) Chen, C.-P.; Luo, C.; Ting, C.; Chuang, S.-C. *Chem. Commun.* **2011**, *47*, 1845.
- (4) (a) Yao, Y.; Hou, J.; Xu, Z.; Li, G.; Yang, Y. *Adv. Funct. Mater.* **2008**, *18*, 1783. (b) Chan, S.-H.; Hsiao, Y.-S.; Hung, L.-I.; Hwang, G.-W.; Chen, H.-L.; Ting, C.; Chen, C.-P. *Macromolecules* **2010**, *43*, 3399. (c) Tsai, J. H.; Lai, Y. C.; Higashihara, T.; Lin, C. J.; Ueda, M.; Chen, W. C. *Macromolecules* **2010**, *43*, 6085.
- (5) (a) Yu, C.-Y.; Chen, C.-P.; Chan, S.-H.; Hwang, G.-W.; Ting, C. *Chem. Mater.* **2009**, *21*, 3262. (b) Peet, J.; Kim, J. Y.; Coates, N. E.; Ma, W. L.; Moses, D.; Heeger, A. J.; Bazan, G. C. *Nat. Mater.* **2007**, *6*, 497. (c) Chen, H.-C.; Wu, I.-C.; Hung, J.-H.; Chen, F.-J.; Chen, I.-W. P.; Peng, Y.-K.; Lin, C.-S.; Chen, C.-H.; Sheng, Y.-J.; Tsao, H.-K.; Chou, P. T. *Small* **2011**, *7*, 1098.
- (6) (a) Radano, C. P.; Scherman, O. A.; Stingelin-Stutzmann, N.; Müller, C.; Breiby, D. W.; Smith, P.; Janssen, R. A. J.; Meijer, E. W. *J. Am. Chem. Soc.* **2005**, *127*, 12502. (b) Li, B.; Sauve, G.; Iovu, M. C.; Jeffries-El, M.

Zhang, R.; Cooper, J.; Santhanam, S.; Schultz, L.; Revelli, J. C.; Kusne, A. G.; Kowalewski, T.; Snyder, J. L.; Weiss, L. E.; Fedder, G. K.; McCullough, R. D.; Lambeth, D. N. *Nano Lett.* **2006**, *6*, 1598. (c) Iovu, M. C.; Craley, C. R.; Jeffries-El, M.; Krankowski, A. B.; Zhang, R.; Kowalewski, T.; McCullough, R. D. *Macromolecules* **2007**, *40*, 4733.

(7) Zhang, Y.; Tajima, K.; Hirota, K.; Hashimoto, K. *J. Am. Chem. Soc.* **2008**, *130*, 7812.

(8) (a) Rajaram, S.; Armstrong, P. B.; Kim, B. J.; Fréchet, J. M. J. *Chem. Mater.* **2009**, *21*, 1775. (b) Kim, B. J.; Kang, H.; Char, K.; Katsov, K.; Fredrickson, G. H.; Kramer, E. J. *Macromolecules* **2005**, *38*, 6106. (c) Lyu, S.; Jones, T. D.; Bates, F. S.; Macosko, C. W. *Macromolecules* **2002**, *35*, 7845. (d) Sivula, K.; Ball, Z. T.; Watanabe, N.; Fréchet, J. M. J. *Adv. Mater.* **2006**, *18*, 206. (e) Lee, J. U.; Jung, J. W.; Emrick, T.; Russell, T. P.; Jo, W. H. *J. Mater. Chem.* **2010**, *20*, 3287.

(9) Miyakoshi, R.; Yokoyama, A.; Yokozawa, T. *J. Am. Chem. Soc.* **2005**, *127*, 17542.

(10) Zhai, L.; Pilston, R. L.; Zaiger, K. L.; Stokes, K. K.; McCullough, R. D. *Macromolecules* **2003**, *36*, 61.

(11) van der Veen, M. H.; de Boer, B.; Stalmach, U.; van de Wetering, K. I.; Hadziioannou, G. *Macromolecules* **2004**, *37*, 3673.

(12) (a) Dante, M.; Yang, C.; Walker, B.; Wudl, F.; Nguyen, T. Q. *Adv. Mater.* **2010**, *22*, 1835. (b) Liu, J.; Sheina, E.; Kowalewski, T.; McCullough, R. D. *Angew. Chem.* **2002**, *114*, 339.

(13) Prosa, T. J.; Winokur, M. J.; Moulton, J.; Smith, P.; Heeger, A. J. *Macromolecules* **1992**, *25*, 4364.

(14) Lu, G.; Li, L.; Yang, X. *Small* **2008**, *4*, 601.

(15) (a) Yang, X.; Lu, G.; Li, L.; Zhou, E. *Small* **2007**, *3*, 611. (b) Li, L.; Tang, H.; Wu, H.; Lu, G.; Yang, X. *Org. Elect.* **2009**, *10*, 1334.

(16) (a) Chen, C.-P.; Chan, S.-H.; Chao, T.-C.; Ting, C.; Ko, B.-T. *J. Am. Chem. Soc.* **2008**, *130*, 12828. (b) Chan, S.-H.; Chen, C.-P.; Chao, T.-C.; Ting, C.; Ko, B.-T. *Macromolecules* **2008**, *41*, 5519.

(17) (a) Reid, O. G.; Munechika, K.; Ginger, D. S. *Nano Lett.* **2008**, *8*, 1602. (b) Melzer, C.; Koop, E. J.; Mihailitchi, V. D.; Blom, P. W. M. *Adv. Funct. Mater.* **2004**, *14*, 865.

(18) (a) R. A. Marsh, R. A.; Groves, C.; Greenham, N. C. *J. Appl. Phys.* **2007**, *101*, 083509–1. (b) Zhao, Y.; Xie, Z.; Qu, Y.; Geng, Y.; Wang, L. *Appl. Phys. Lett.* **2007**, *90*, 043504.

(19) Schilinsky, P.; Waldauf, C.; Hauch, J.; Brabec, C. J. *J. Appl. Phys.* **2004**, *95*, 2816.

(20) Liu, W.; Liu, R.; Wang, W.; Li, W.; Liu, W.; Zheng, K.; Ma, L.; Tian, Y.; Bo, Z.; Huang, Y. *J. Phys. Chem. C* **2009**, *113*, 11385.